frontiers | Frontiers in Marine Science

TYPE Original Research
PUBLISHED 29 January 2025
DOI 10.3389/fmars.2025.1471650

OPEN ACCESS

EDITED BY
Daniel Puppe,
Leibniz Center for Agricultural Landscape Research (ZALF), Germany

REVIEWED BY
Yongquan Yuan,
Chinese Academy of Sciences (CAS), China
Bin Zhao,
Ministry of Natural Resources, China

*CORRESPONDENCE
Bin Wang
wangbin@sio.org.cn
Hongliang Li
lihongliang@sio.org.cn

RECEIVED 28 July 2024
ACCEPTED 09 January 2025
PUBLISHED 29 January 2025

CITATION
Liu X, Wang B, Chen S, Jin H, Zhuang Y, Jiang Z, Li H and Chen J (2025) The size-fractionated composition of particulate biogenic silica and its ecological significance in the Changjiang Estuary area.
Front. Mar. Sci. 12:1471650.
doi: 10.3389/fmars.2025.1471650

The size-fractionated composition of particulate biogenic silica and its ecological significance in the Changjiang Estuary area

Xizhen Liu[1,2], Bin Wang[2,3]*, Siyang Chen[1], Haiyan Jin[2,4], Yanpei Zhuang[5], Zhibing Jiang[2], Hongliang Li[2,4]* and Jianfang Chen[2,4]

[1]Marine Monitoring and Forecasting Center of Zhejiang Province, Hangzhou, China, [2]Key Laboratory of Marine Ecosystem Dynamics, Second Institute of Oceanography, Ministry of Natural Resources, Hangzhou, China, [3]Donghai Laboratory, Zhoushan, China, [4]State Key Laboratory of Satellite Ocean Environment Dynamics, Second Institute of Oceanography, Ministry of Natural Resources, Hangzhou, China, [5]Polar and Marine Research Institute, Jimei University, Xiamen, China

The concentrations and distributions of particulate biogenic silica (PBSi) and its size-fractionated composition (>20 μm, 0.8–20 μm) of the Changjiang Estuary and its adjacent area were investigated during the summer of 2011. PBSi, primarily produced by diatoms in the surface waters of oceans, was examined for correlations with hydrographic conditions, nutrients, particulate organic carbon, and dissolved oxygen. The distribution of PBSi showed distinct patterns: high levels in nearshore, but relatively low further offshore; low concentrations in the surface layer, whereas relatively high concentrations in the bottom layer. Large-sized PBSi (>20 μm) prevailed in the surface layer, whereas small-sized PBSi (0.8–20 μm) dominated in the bottom layer. Temperature and nutrients were crucial factors controlling the grain size structure and distribution of PBSi. Further, we observed that the distinct zones of high PBSi values in the surface waters were affected by the Changjiang freshwater flushing, and those in the bottom waters were affected by the Yellow Sea Cold Water masses. Moreover, in the area where >20-μm PBSi prevailed, the silicate-to-nitrate ratio was less than 1 at most sampling stations, rendering silicate the limiting nutrient in this area. The PBSi/particulate organic carbon values in the surface waters of the study area ranged from 0.01 to 0.3. Areas exhibiting values exceeding 0.13 primarily clustered in nearshore waters, which was characterized by a dominance of large-sized (>20 μm) PBSi. The nearshore benthic waters exhibited anoxic conditions, where diatoms predominantly comprised the phytoplankton biomass and organic matter featured marine phytoplankton. Consequently, the proliferation of diatoms (siliceous phytoplankton) in the midupper water significantly contributed to the hypoxic conditions at the bottom, as diatoms underwent dissolution during sedimentation, leading to oxygen depletion.

KEYWORDS

Changjiang Estuary, particulate biogenic silica, size-fractionated composition, particulate organic carbon, hypoxia

1 Introduction

Diatoms play an important role in the marine biological pump process, contributing approximately 30% of global oceanic primary productivity (Nelson et al., 1995; Tréguer et al., 1995) and up to 75% in nearshore and eutrophic water (Liu et al., 2008). Biogenic silica (BSi) is produced in the surface waters of oceans, mostly by diatoms, but also by radiolarians and silicoflagellates (Nelson et al., 1995). The particulate biogenic silica (PBSi) in the water column represents the standing stock of BSi in the photic zone and can be used as an indicator of the instantaneous biomass of siliceous phytoplankton (Nelson et al., 2002).

The marginal sea is the main place of BSi burial and transformation and the main reservoir of BSi in the ocean, and it plays an important role in the global biogeochemical cycle of silica (Conley, 1997). As one of the most crucial estuarine-marginal sea regions worldwide, the Changjiang Estuary and its adjacent waters are the ideal place to study the distributional characteristics of BSi and its ecological effects. This is because of the unique hydrographic characteristics and abundant nutrient inputs. Diatoms dominate biomass over the East China Sea (ECS), particularly during the summer months, because of the Changjiang plume. The presence of diatom blooms resulted in significantly higher concentrations of PBSi in the surface layer in summer than in other seasons (Cao et al., 2013). The biogenic organic particulate matter from the upper layers of the water column is transformed, degraded, settled, and buried in the ocean sediments by the action of a silicate pump (Buesseler et al., 2001). The biogeochemistry of Si in the marine environment is of global significance. Further, the behavior of Si can be used as a proxy to understand the carbon cycle in the ocean, which drives the biological pump in the water column (Tréguer and Pondaven, 2000).

The BSi content of different size fractions varies significantly in ECS as it is largely controlled by the species of diatoms and their cell sizes. Thus, the grain size distribution of the bulk sediment should be considered when using BSi as a proxy for the primary production of diatom (Wang et al., 2014). The size-fractionated composition of PBSi is an important factor controlling the particulate organic carbon in marine areas where diatoms are the dominant population, and it is a good indicator of the biological pump efficiency in this area. However, the previous studies on ECS are mainly about the concentration of PBSi in water column and BSi in sediments (Liu et al., 2005; Wang et al., 2014; Li et al., 2018). Studies on the contribution of PBSi with different sizes of the standing stock of BSi in water columns and the ecological significance of the size-fractionated composition of PBSi are very limited. The occurrence of hypoxia off the Changjiang Estuary during summer can be traced back to the 1950s (Li et al., 2002), and the expansion of the affected area has been documented (Li et al., 2002; Zhu et al., 2011). Seasonal hypoxia off the Changjiang Estuary is an increasingly recognized environmental issue of global concern to both the scientific community and the public. It is caused by the decomposition of newly produced marine and riverine-borne biogenic substances deposited in the bottom water (Chen et al., 2007). Therein, marine-sourced organic matter is the dominant oxygen consumer in the subsurface hypoxia zone (Wang et al., 2016). Diatoms typically prevail in the phytoplankton community of nutrient-rich aquatic environments (Nelson et al., 1995; Tréguer and Pondaven, 2000). However, they exhibit rapid reproduction and opportunistic behavior, thriving in relatively cool temperatures (<20°C) and areas with turbulent mixing (Lomas and Glibert, 1999). Therefore, the factors affecting the distribution of BSi and the relationship between BSi and hypoxia formation are of equal interest. This article elucidates the size-fractionated composition of PBSi in the water column, its influencing factors, its relationship with particulate organic carbon (POC), and the formation of a hypoxia zone. Further, this study provides insights into the size-fractionated (>20 μm, 0.8–20 μm and total) composition of PBSi in the ECS and its biogeochemical cycling processes.

2 Materials and methods

2.1 Study site

The Changjiang Estuary and its adjacent area are among the most crucial estuarine-coastal ocean continuum worldwide. The region's water system is complex, including the cold, fresh, and nutrient-rich Changjiang Diluted Water and ECS Coastal Water; the warm and nutrient-poor Taiwan Warm Water Current and Kuroshio Water; and the relatively cold, fresh, and nutrient-rich Yellow Sea Coastal Water and the Yellow Sea Cold Water Mass (Zhang et al., 2007; Chen, 2009). During summer, southwest winds prevail and the Changjiang Diluted Water extends northeast toward the Tsushima/Korea Straits (Beardsley et al., 1985; Liu et al., 2016a). Extensive water exchange between the ECS and Kuroshio occurs across the shelf break through upwelling and frontal processes. The incursion of the Kuroshio sustains the upwelling conditions, which are enhanced by the summer southerly winds (Su, 1998; Zhang et al., 2007).

2.2 Sample collection

This study was conducted from July 5 to July 25, 2011, onboard the scientific research vessel Dongfanghong 2 of the Ocean University of China for *in situ* observations in the Yellow Sea and ECS. As shown in Figure 1, three sections (D, F, and PN) were investigated from the Changjiang Estuary to the outer shelf area. Water samples were collected using a precalibrated conductivity, temperature, and depth sensors unit (Sea-Bird Electronics, SBE-911 Plus) attached to 12-L Niskin bottles. After seawater was collected, 0.5–2.0 L of seawater was filtered through a 20-μm pore-size nylon membrane to obtain PBSi samples with particle sizes of >20 μm. Subsequently, the seawater was filtered through a 0.8-μm pore-size polycarbonate membrane to obtain PBSi samples with particle sizes ranging from 0.8 to 20 μm. Nutrient samples were filtered through precleaned cellulose acetate membranes (47 mm, pore size 0.45 μm), and 0.3 mL of 35 g/L $HgCl_2$ was added into each 100 mL sample to preserve the samples for further analysis.

For POC and POC stable carbon isotope ($\delta^{13}C$) collection, 0.5–2.0 L of seawater was filtered using GF/F filters (47 mm, pore size 0.7 μm) that had been precombusted for 4 h at 450°C. For the

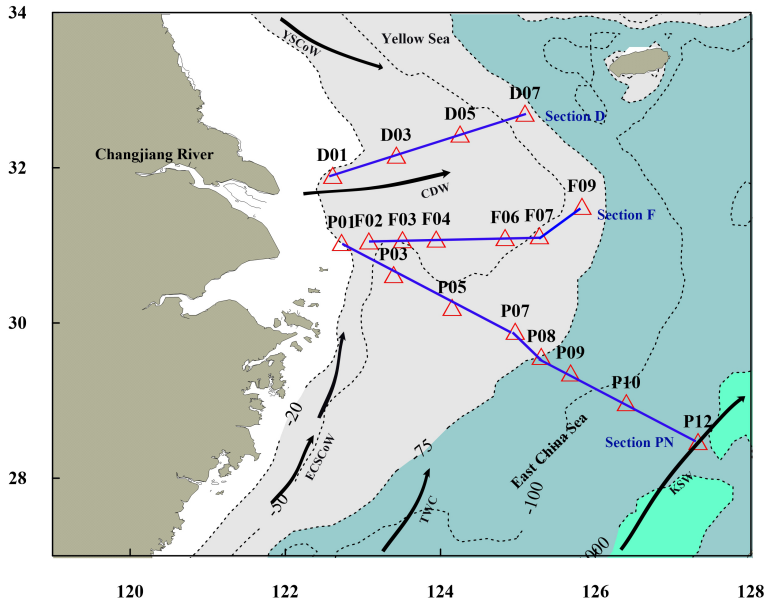

FIGURE 1
The distribution of sampling stations and current systems in the investigated sea area, where CDW is the Changjiang Diluted Water, TWC is the Taiwan Warm Current, ECSCoW is the East China Sea Coastal Current, YSCoW is the Yellow Sea Coastal Water, and KSW is the Kuroshio Surface Water.

Chlorophyll *a* (Chl *a*) collection, 150 mL of seawater was filtered through GF/F membrane filters under low pressure and dim light.

2.3 Analytical methods

Seawater temperature and practical salinity scale (without units) were measured *in situ* using the conductivity, temperature, and depth sensors. The samples for dissolved oxygen (DO) analyses were collected, fixed, and titrated onboard, following the classic Winkler titration procedure (Bryan et al., 1976). The precision of the DO measurements was ±0.02 mg/L.

The PBSi concentrations in the water were determined using the extraction method of Ragueneau et al. (2005). The filters were dried at 60°C and extracted twice with 4 mL of 0.2 mol/L NaOH in polyethylene centrifuge tubes at 100°C for 40 min two times. After centrifugation (3,036.8 × g), the concentrations of Si and Al in the supernatant were determined for both the first step ($[Si]_1$ and $[Al]_1$) and the second step ($[Si]_2$ and $[Al]_2$). Silicate concentration was determined by spectrophotometry using a continuous nutrient flow analyzer (model Skalar San++, Skalar, Holland; Grasshoff et al., 2009), and Al concentration was measured on a Varian Vista Pro inductively coupled plasma atomic emission spectrometer. Since all BSi were extracted in the first step, the $[Si]_2$:$[Al]_2$ ratio was specific to the sample's suspended silicate minerals. The accurate BSi concentration could be calculated using the following formula:

$$PBSi = [Si]_1 - [Al]_1 \times [Si]_2 : [Al]_2 \quad (1)$$

Nitrate and silicate concentrations were determined using a colorimetric method with a Skalar nutrient flow analyzer (Grasshoff et al., 2009). Meanwhile, nitrite, ammonium, and phosphate concentrations were determined manually *in situ* according to standard methods using a spectrophotometer (model 723, Shanghai Jingke, China). The data quality was monitored by intercalibration, and the detection limits for nitrate, nitrite, ammonium, phosphate, and silicate were 0.1, 0.05, 0.05, 0.03, and 0.1 μmol/L, respectively.

The filters for detecting POC and $\delta^{13}C$ were dried at 50°C until constant weight; thereafter, they were decarbonated by fumigating with hydrochloric acid. Carbon concentrations were analyzed using an Elementar Vario MICRO cube elemental analyzer, and $\delta^{13}C$ was analyzed using a Thermo MAT 253 isotope ratio mass spectrometer. Chl *a* data were provided by Yuming Cai (personal communication, 2011). Further, filtered phytoplankton was jammed and extracted with 90% acetone overnight; thereafter, fluorescence was measured using a Turner Designs model 10.

The relationships between PBSi and other variables (e.g., POC and DO) were assessed using correlation analysis. Spearman's rank correlation was applied to evaluate the relationship between PBSi and POC, as it is suitable for non-normally distributed data and can effectively capture non-linear correlations. The relationship between PBSi and DO was examined using a logarithmic regression model, and the coefficient of determination (R^2) and p-value were calculated to assess the model's goodness of fit. To compare the differences in temperature, salinity, nitrate, phosphate, silicate, N/P and silicate/nitrate ratios, DO, and POC between two depth layers (above 10 m and below 10 m) across the three regions (I, II, and III), statistical tests were selected based on data distribution. For datasets that met the assumptions of normality and homoscedasticity, the independent samples t-test was used. For datasets that did not meet these assumptions, the non-parametric Mann-Whitney U test was employed. Additionally, to compare the distribution of PBSi

concentrations in different size fractions (<20 μm and 0.8–20 μm) among regions I, II, and III, as well as the total PBSi distribution between surface and bottom layers, the same statistical approach was applied. The significance level was set at $p < 0.05$, with statistical significance denoted as follows: *$p < 0.05$, **$p < 0.01$, and ***$p < 0.001$, while 'ns' indicated no significant difference. All statistical analyses were conducted using SPSS Statistics 27.

3 Results

3.1 Hydrographic conditions

The temperature and salinity in the study region ranged from 10.4°C to 28.9°C and 16.1 to 34.8, respectively. According to the temperature–salinity analysis of the investigated area, five water masses in the study area were identified (Figure 2A), which were similar to those described in previous studies (Chen, 2009; Zhang et al., 2007). They include (1) Changjiang Diluted Water, with salinities of 22.0–31.0 and temperatures of 20.0°C–30.0°C, (2) Taiwan Warm Current Water, with characteristic salinities of 31.0–34.0 and temperatures of 25.0°C–30.0°C, (3) Shelf Mixed Water (SMW), with salinities of 31.0–34.0 and temperatures of 15.0°C–25.0°C, (4) Yellow Sea Cold Water, with salinities of 31.0–34.0 and temperatures of 10.0°C–15.0°C, and (5) Kuroshio Surface with salinities of 34.0–35.0 and temperatures of 22.5°C–28.0°C. The investigated area was divided into three parts based on the characteristics of different water masses (Figure 2B). Region I was mainly affected by the Changjiang Diluted Water, and Region II was affected by the relatively low-temperature and moderately saline SMW and Yellow Sea Cold Water Mass. Region III was mainly affected by the high-temperature and highly saline Taiwan Warm Current and the Kuroshio surface water, which included the stations east of P05 in Section PN. Owing to the big difference in the temperature and salinity of the surface and bottom waters in the investigated area in summer, as shown in Figure 2, the temperature and salinity characteristics of the waters above 10 m and waters below 10 m were divided and further analyzed to obtain the following results. For Region I, the salinity of the water column above 10 m was <31, which was the characteristic value of the Changjiang Diluted Water. The water column below 10 m was caused by the water masses of the Changjiang Diluted Water, the coastal current of the Yellow Sea, and the Taiwan Warm Current, which defined the SMW (Zhang et al., 2007). For Region II, the water column above 10 m showed the thermohaline characteristics of SMW. Further, the temperature of the water column below 10 m was significantly low, all less than 15°C, under the influence of the expansion of the Yellow Sea Cold Water Masses to the south in summer. In Region III, the waters above 10 m were mainly affected by the Taiwan Warm Current with high temperature and subhigh salinity characteristics. Furthermore, the deep waters below 10 m with high salinity characteristics could result from the intrusion of Kuroshio Surface Water (Zhou et al., 2018).

3.2 Distribution of seawater constituents

The distributions of DO in surface and bottom water are shown in Figure 3. A bottom hypoxia area (with DO concentration less than 3 mg/L) was found near the mouth of the Changjiang, centered at station P01 (St.P01, DO = 2.6 mg/L) and station F02 (St.F02, DO = 3.0 mg/L). However, this region did not exhibit high values of surface DO, with areas of high surface values occurring in St.D03 (DO = 8.4 mg/L) and

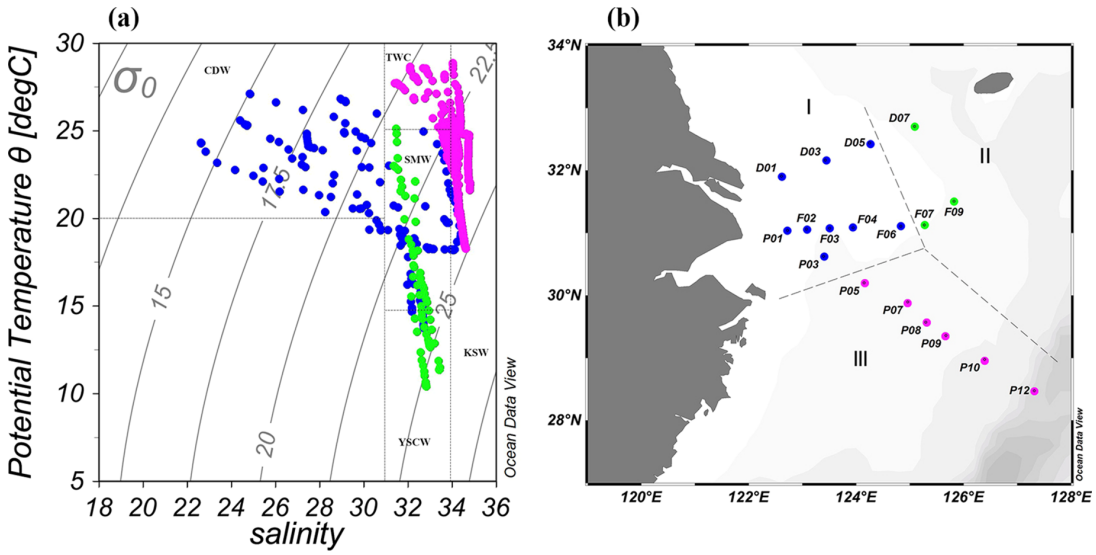

FIGURE 2
Scatter plot of potential temperature *vs.* salinity **(A)** and spatial division of the investigated area based on water mass characteristics **(B)**. **(A)** The scatter plot illustrates the characteristics of different water masses: CDW (Changjiang Diluted Water), TWC (Taiwan Warm Current), SMW (Shelf Mixed Water), YSCW (Yellow Sea Cold Water Mass), and KSW (Kuroshio Surface Water). The colors represent the spatial divisions: blue corresponds to Region I, green corresponds to Region II, and red corresponds to Region III. **(B)** The investigated area is divided into three regions based on water mass characteristics: Region I, Region II, and Region III. The station colors are consistent with panel **(A)**: blue represents Region I stations, green represents Region II stations, and red represents Region III stations.

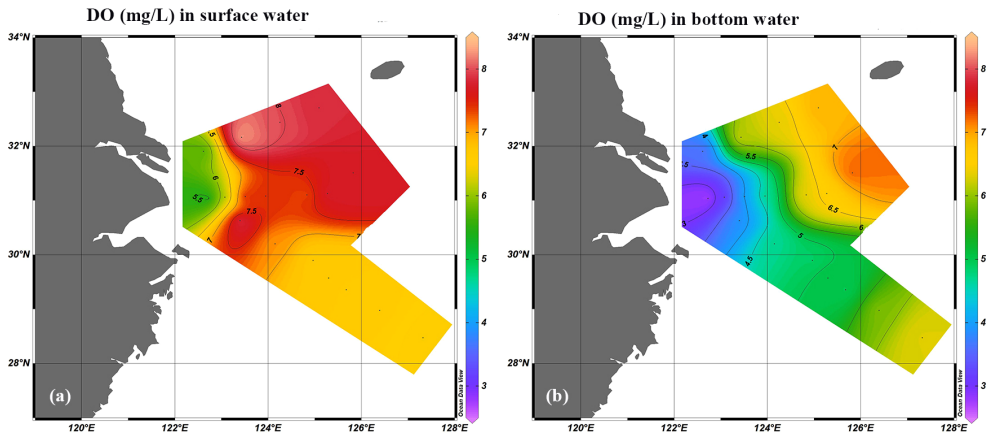

FIGURE 3
Distribution of dissolved oxygen concentration (mg/L) in the surface **(A)** and bottom **(B)** waters of the investigated area.

St.D05 (DO = 8.0 mg/L). Due to sampling limitation, the surface DO sample for St.F02 was not obtained; therefore, the DO value of the 10 m layer at this specific station is depicted in Figure 3A. The surface POC concentration showed a large variation, ranging from 2.0 to 20.1 µmol/L (8.6 ± 6.3 µmol/L, mean ± standard deviation, as used hereinafter) (Figure 4A). Two areas of relatively high POC concentrations were observed: the northern part outside the Changjiang Estuary was at St.D01 (POC = 26.0 µmol/L) and St.F02 (POC = 20.1 µmol/L), whereas the southern part was at St.P05 (POC = 13.8 µmol/L). In the vast majority of stations, the bottom POC values were greater than the surface values, ranging from 1.7 to 154.9 µmol/L (24.7 ± 38.0 µmol/L, Figure 4B). Furthermore, DO and POC concentrations were calculated across the three regions (Table 1). The results revealed that DO levels were generally lower in deeper waters (below 10 m), with the most pronounced decrease observed in Region I. In contrast, POC concentrations exhibited high variability, with a significant increase in bottom waters of Region II, likely due to sediment resuspension or organic matter accumulation. This study examined nutrient concentrations in the upper and lower water column and analyzed them according to the various regions, as shown in Table 1. In the upper water column, nitrate concentration decreased offshore, with high concentration in Region I and low concentrations in Regions II and III. As the depth increased, nitrate levels decreased in Region I, whereas they increased in Regions II and III. The minimum average concentration for phosphate was observed in the water column below 10 m in Region II. Meanwhile, the average phosphate levels in the water column from other regions varied slightly. The nearshore exhibited higher silicate concentrations in Region I, with mean values of 19.0 µmol/L and 21.1 µmol/L in the upper and lower waters, respectively, than in Regions II and Region III.

3.3 Characteristic of particulate biogenic silica distribution and size-fractionated compositions

The PBSi concentration in the surface layer ranged from 0.01 to 2.3 µmol/L (Figure 5A), with a mean concentration of 0.7 ± 0.8 µmol/L.

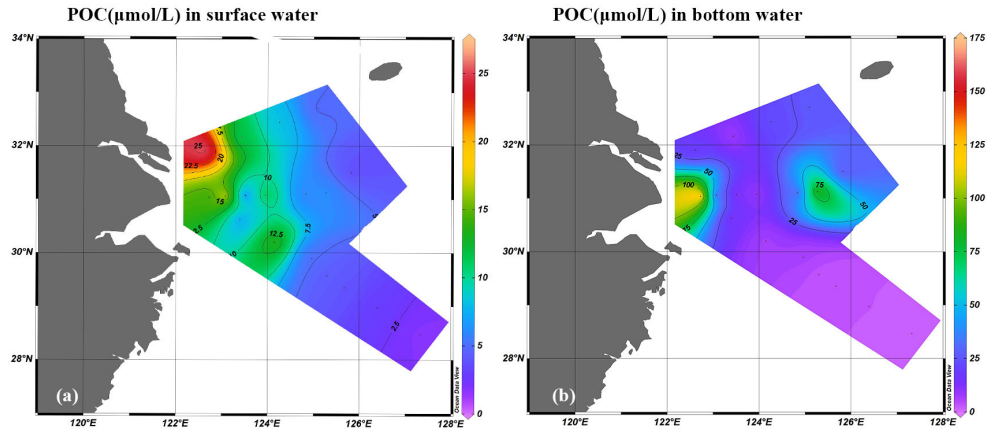

FIGURE 4
Distribution of the particulate organic carbon (POC) concentration (µmol/L) in the surface **(A)** and bottom **(B)** waters of the investigated area.

TABLE 1 Temperature (°C), salinity, nutrient concentrations (μmol/L), and nutrient ratios in the water column at different depths of the investigated area.

Water column	Temperature	Salinity	Nitrate	Phosphate	Silicate	N/P	Silicate/ nitrate	DO	POC
I (above 10 m)	23.8 ± 2.0	27.9 ± 2.7	18.7 ± 10.0	0.4 ± 0.3	19.0 ± 11.1	92.0 ± 74.6	1.0±0.4	6.9±1.5	11.1±5.8
I (below 10m)	18.1±2.1***	33.0±1.3***	12.7±3.5*	0.8±0.5**	21.1±5.0ns	22.9±13.8***	1.7±0.3***	4.6±1.4***	25.0±39.5ns
II (above 10 m)	22.3 ± 1.6	31.8 ± 0.4	0.9 ± 0.4	0.03 ± 0.05	10.9 ± 1.4	21.5 ± 8.7	13.7±4.9	7.9±0.3	4.8±0.8
II (below 10m)	12.8±3.1***	32.9±0.4***	10.1±2.9***	0.5±0.2**	16.7±1.5***	33.5±26.7ns	1.8±0.6***	7.2±0.5**	32.8±33.7**
III (above 10 m)	28.3 ± 0.5	32.7 ± 0.8	0.8 ± 0.5	0.2 ± 0.2	3.8 ± 1.6	17.1 ± 7.4	22.2±55.3	6.7±0.2	5.3±3.9
III (below 10m)	22.7±3.2***	34.2±0.5***	4.0±3.0**	0.4±0.3**	10.3±6.3**	15.7±14.8ns	4.0±3.1ns	5.8±0.8**	4.1±1.8ns

The numbers in the table represent the quantitative data as mean ± standard deviation (SD).
***p < 0.001, **p < 0.01, *p < 0.05, ns, no statistical significance.

The peak concentration of 2.3 μmol/L was recorded at St.P05, whereas the second highest concentration of 2.1 μmol/L was observed at St.F02, located at the mouth of the Changjiang. The levels of PBSi maxima were comparable to those of previous studies in the region (Liu et al., 2005). These two stations showed a dominance of PBSi in the >20-μm size fraction, representing 69.7% and 79.4% of the total PBSi concentration, respectively. The PBSi concentration in the bottom layer ranged from 0.05 to 6.8 μmol/L (Figure 5B), with a mean concentration of 2.0 ± 2.1 μmol/L. The highest and second highest values of 6.8 and 6.2 μmol/L in the bottom layer were observed at stations D05 and D07, which were offshore and dominated by the PBSi of the 0.8–20 μm size fraction. Further, they accounted for 73.6% and 84.6% of the total PBSi concentration, respectively. Additionally, the bottom PBSi concentration at nearshore St.P01 was relatively high, at 5.6 μmol/L, showing a predominance of the >20- μm size fraction, representing 85% of the total PBSi concentration. The lowest concentrations in the surface and bottom layers were determined at offshore St.P12. Overall, the distribution of the surface PBSi showed a pattern of high concentration near the coast and low concentration further offshore, with high values concentrated in the Changjiang Estuary area. The bottom PBSi concentration was higher than that of the surface layer, and the high-value area in the bottom layer was concentrated in the offshore D05 area and the nearshore P01 area. Significant differences ($p<0.05$) were observed between the bottom PBSi and the surface PBSi. For size-fractionated compositions, in surface waters, the PBSi concentration in the >20-μm size fraction ranged from 0.004 to 1.7 μmol/L, accounting for 0.5% to 84.4% of the total PBSi, with an average proportion of 51.2%. In the bottom waters, the PBSi concentration in the 0.8–20 μm size fraction ranged from 0.01 to 5.3 μmol/L, accounting for 11.2% to 98.5% of the total PBSi, with an average proportion of 66.3%. Overall, the large-particle-size PBSi (>20 μm) predominated in the surface layer, accounting for 55.6% of the survey stations, primarily concentrated in the Changjiang Estuary. For the offshore area, the predominance of the large-particle-size PBSi gradually decreased, and the small-particle-size PBSi (0.8–20 μm) predominated in the bottom layer, accounting for 72.2% of the survey stations.

In Section D, the concentration of PBSi in the >20-μm size fraction ranged from 0.01 to 1.8 μmol/L, with an average value of 0.4 ± 0.5 μmol/L, accounting for 24.7% of the total PBSi on average. Further, the PBSi concentration of particle size 0.8–20 μm ranged from 0.08 to 5.3 μmol/L, with an average value of 1.6 ± 1.9 μmol/L, accounting for 75.3% of the total PBSi on average (Figure 6A). We found that in the majority of stations in Section D, the PBSi of particle size 0.8–20 μm dominated. In Section F, the concentration of PBSi in the >20-μm size fraction at all depths was in the range of 0.003–0.8 μmol/L, with an average value of 0.3± 0.5 μmol/L, accounting for 44.6% of the total PBSi on average. The concentration of PBSi in the 0.8–20 μm size fraction ranged from 0.02 to 2 μmol/L, with an average value of 0.4 ± 0.5 μmol/L, accounting for 55.4% of the total PBSi on average (Figure 6B). We found that in Section F, the PBSi concentration in the 0.8–20 μm size fraction was higher than that in the >20-μm fraction. However, the dominance of the PBSi in the >20-μm size fraction was concentrated in the surface and middle waters, and this dominance weakened with the increase in the depth of the water column. In Section PN, the concentration of PBSi in the >20-μm size fraction at each depth ranged from 0.004 to 8.4 μmol/L, with an average value of 0.7 ± 1.8 μmol/L. It accounted for 0.4% to 88.8% of the total PBSi, with an average of 43.0%, and the >20-μm PBSi size fraction dominated mainly in the surface water of the frontal zone at stations P03 and P05 (Figure 6C). The concentration of PBSi in the 0.8–20 μm size fraction ranged from 0.01 to 9.6 μmol/L, with an average value of 0.9 ± 2.1 μmol/L, and the proportion of the total PBSi ranged from 11.2% to 99.6%, with an average of 57.0%. We considered that the PBSi in the 0.8–20 μm size fraction was dominant, concentrating in the surface and middle water column at nearshore station P01 and in the bottom water column at most other stations. Furthermore, we calculated the size-fractionated PBSi concentration across the three regions (Figure 7). Region I and Region II exhibited higher PBSi levels in the 0.8–20 μm size fraction compared to >20-μm fraction, while Region III showed minimal differences between the two size fractions. In Region I, there was a significant difference ($p<0.05$) in PBSi concentration between 0.8–20 μm and >20-μm, whereas in Regions II and III, there was no statistical significance.

4 Discussion

4.1 Factors affecting the distribution of particulate biogenic silica

The concentrations of PBSi ranged from 0.01 to 18.03 μmol/L, with an average concentration of 1.3 ± 2.6 μmol/L. These values were

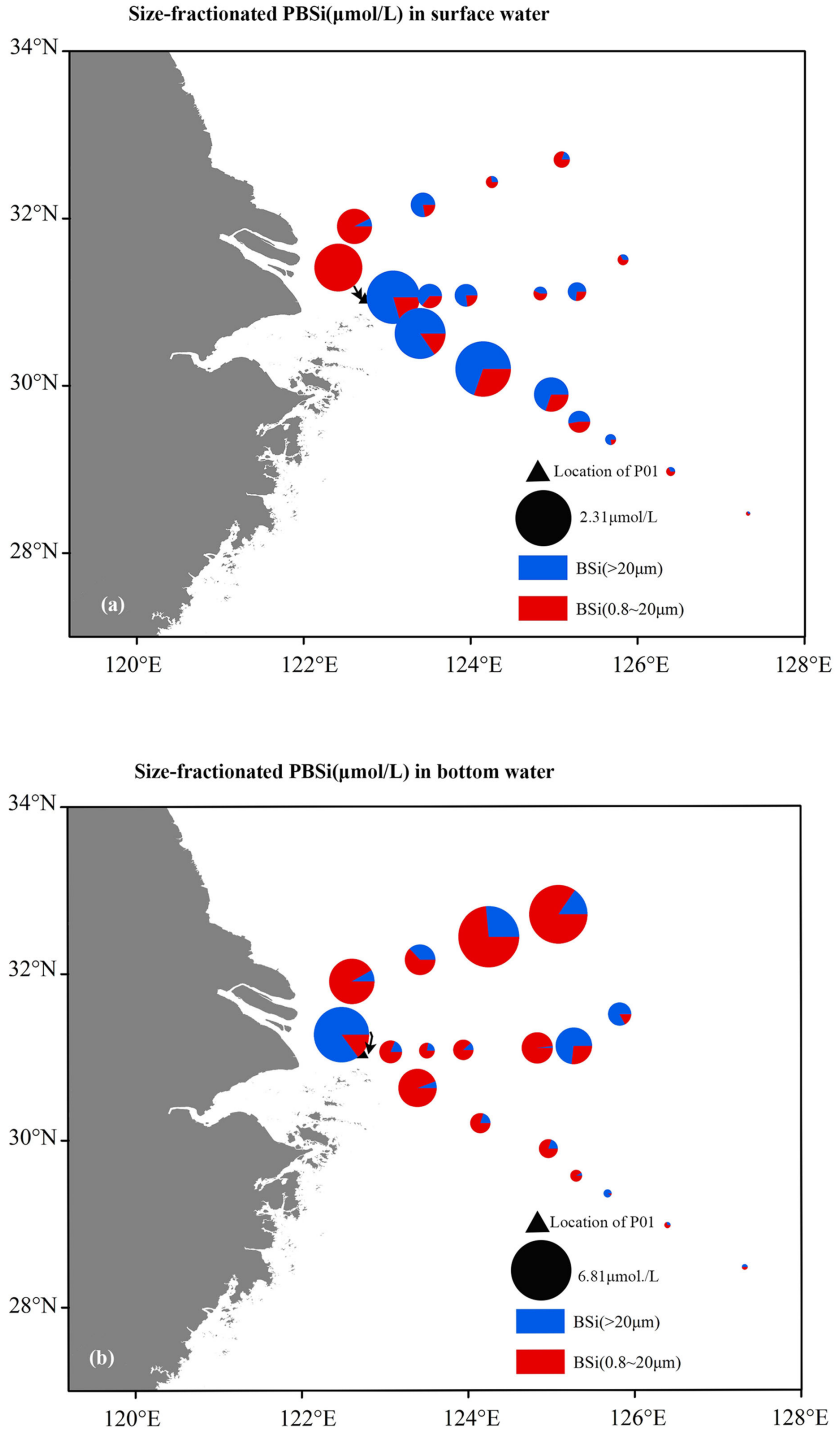

FIGURE 5
Distribution of the particulate biogenic silica (PBSi) concentration (μmol/L) in different size fractions in the surface **(A)** and bottom **(B)** waters of the investigated area. The triangle indicates the location of Station P01, and the pie chart marked by an arrow indicates the size-fractionated PBSi concentration (μmol/L) in Station P01.

comparable to those observed in the Bohai Sea and Yellow Sea during spring (1.1 ± 1.4 μmol/L) but lower than the concentrations recorded in the Bohai Sea and Yellow Sea during autumn (2.6 ± 2.1 μmol/L) (Liu et al., 2016b). To analyze the influence of different water masses on PBSi distribution, we calculated temperature, salinity, nitrate, phosphate, silicate, as well as N/P and silicate/nitrate ratios in the surface waters (0-10 m) and bottom waters (>10 m depth to the seabed) across the three regions (Table 1). Except for silicate in Region I, N/P ratios in Region II and III, and silicate/nitrate ratios in Region III, all other parameters showed significant differences between depths. High values of surface PBSi were mainly concentrated in Region I. Region I is affected by the diluted water

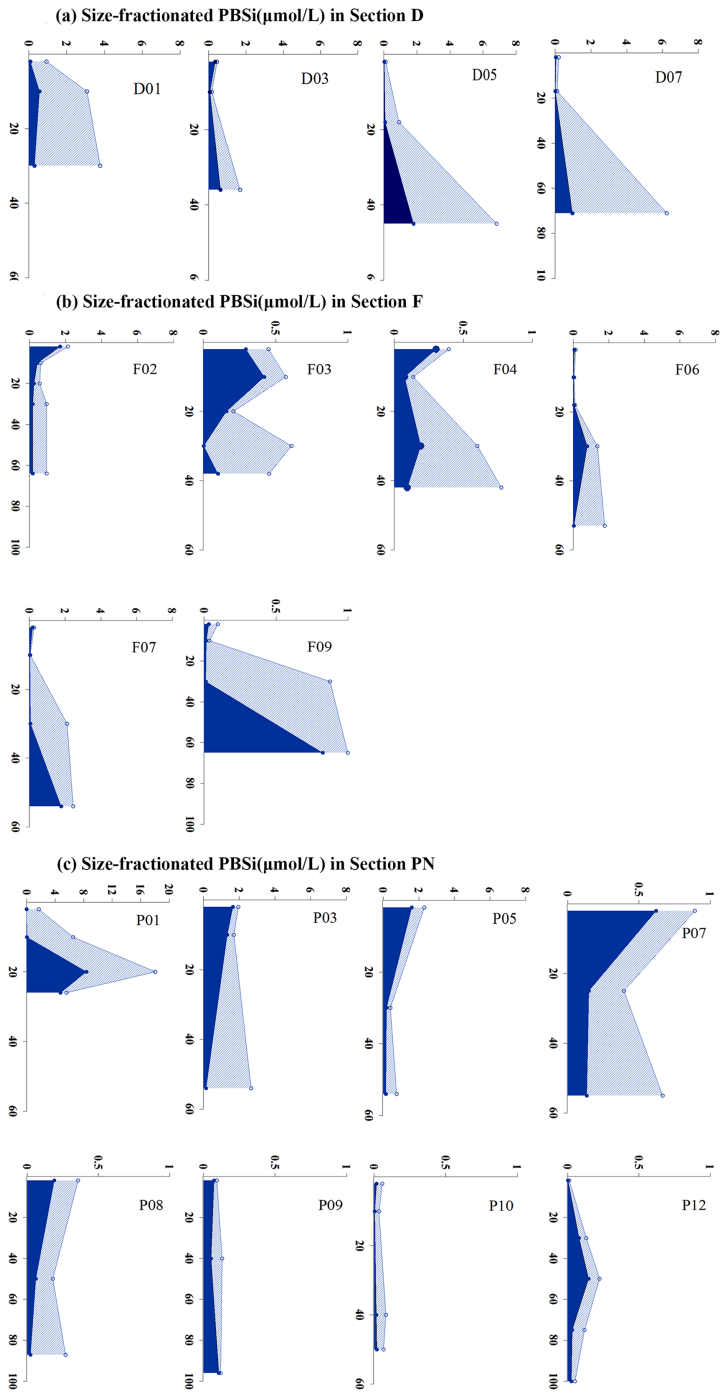

FIGURE 6
Distribution of PBSi concentration (μmol/L) in different size fractions in Sections D **(A)**, F **(B)**, and PN **(C)** of the investigated area. The dark blue shading indicates the PBSi concentration in the >20-μm size fraction, whereas the stripes indicate the PBSi concentration in the 0.8–20 μm size fraction.

from the Changjiang, which brings abundant nutrients to the ECS, thereby providing favorable conditions for the growth of diatoms. Freshwater inputs might contribute to the development of high PBSi values. Further, Conley (1997) reported that the PBSi levels in the world's rivers, including the Amazon, Mississippi, and Congo, ranged from (2.7 ± 0.52) to (74 ± 17.60) μmol/L, with an average level of 28 μmol/L. Diatoms thrive in nearshore waters, and compared with dinoflagellates, diatoms thrive better in environments with low salinity, turbidity, and high nutrients (Jiang et al., 2015). In circumstances of sufficient nutrients, diatoms have a competitive growth advantage, whereas in situations of insufficient nutrient supply later on, the growth of motile large dinoflagellates takes precedence (Savidge et al., 1995). The growth of diatoms depends not only on nitrate and phosphate but also on the supply of

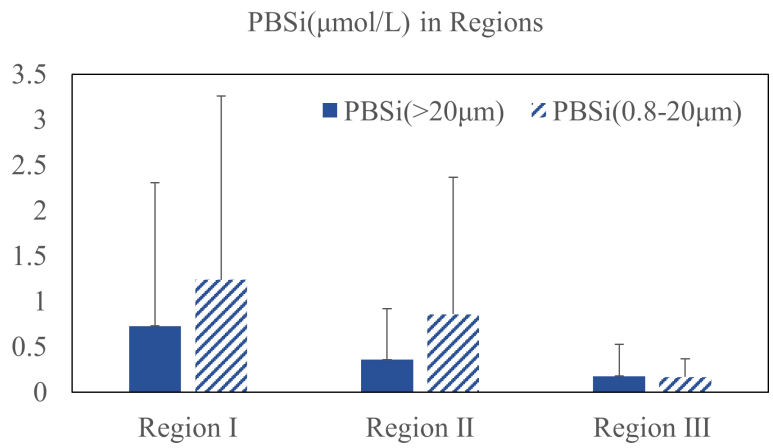

FIGURE 7
Distribution of PBSi concentration (μmol/L) in different size fractions across Regions I, II, and III. The dark blue bars represent the PBSi concentration in the >20-μm size fraction, while the striped bars represent the PBSi concentration in the 0.8–20 μm size fraction.

monomeric silicic acid, which can be used for building up frustules consisting of amorphous silica. In this area, the concentrations of nitrate and silicate reached 18.7 ± 10.0 and 19.0 ± 11.1 μmol/L, respectively, providing sufficient nutrients for diatom growth. In the bottom water of Region II, a high-value area of PBSi was measured because of the summer-extended Yellow Sea Cold Water Mass, lowering the water temperature to below 15°C, which diatoms prefer for growth (Xiao et al., 2018). In the surface water of Area II, the temperature was similarly lower than that in the other two areas. Under low-temperature conditions, diatom cells successfully divide by developing a tree-like pattern (low silicification), affording high cell density (Javaheri et al., 2015). As the temperature increases, the algal community shifts from a typical community with both diatoms and dinoflagellates to a community dominated by micro-flagellates (Anderson et al., 1994).

From the perspective of size-fractionated compositions, PBSi in the 0.8–20 μm size fraction predominantly existed in the D, F, and PN sections overall. However, the >20-μm PBSi size fraction predominated in the surface and middle waters in the nearshore of Section F and PN (i.e., region I). Previous studies have shown that the nano-diatoms are the dominant species in ECS, with dominant cells of 2–14 μm, resulting in a high BSi content in fraction <16 μm (Wang et al., 2014). The convergence of the Taiwan Warm Current and freshwater results in water stratification. Coastal and offshore water systems play a crucial role in controlling the composition of phytoplankton particle sizes (Ho et al., 2015). Small phytoplankton species tend to dominate in the low-nutrient regions of the ocean, whereas large species tend to thrive in nutrient-rich waters (Maranon et al., 2001; Li, 2002; Kostadinov et al., 2010). Chain-formed, small-sized (<20 μm) diatoms have a relatively high surface-area-to-volume ratio, facilitating the absorption of nutrients, particularly phosphates (Karp-Boss et al., 1996). The ratio at which phytoplankton absorb nitrogen and phosphorus nutrients is 16:1 (Redfield ratio), and phosphorus is a limiting factor that influences phytoplankton growth in most parts of the ECS (Harrison et al., 1990). The ratio of silicate to nitrogen required for diatom growth is conventionally close to 1 (Brzezinski, 1985). However, nitrates are depleted first in waters where the silicate/nitrate ratio is >1, and silicates are depleted first in waters where the ratio is <1 (Levasseur and Therriault, 1987). In our research, most stations had a silicate/nitrate ratio of <1 in the region where PBSi larger than 20 μm dominated, making silicate the limiting factor. The growth of diatoms requires monomeric silicic acid to synthesize their frustules, indicating that the diatoms with large individuals (>20 μm) have a relatively high demand for silicate. However, the region is rich in nutrients with nitrate and silicate, which can provide essential nutrients for the growth of large-sized PBSi. However, as diatoms proliferate further, silicate might be depleted first.

4.2 Relationship between particulate biogenic silica and particulate organic carbon

The primary mechanism for ocean carbon storage is the action of the "biological pump." Diatoms are the most significant contributors to global marine primary productivity, and their growth process involves the utilization of dissolved silica to synthesize their siliceous shells. Thus, the "biological carbon pump" in the ocean is mainly driven by the "biological silica pump." Without silicate limitation, 27 marine diatom cultures yielded an average BSi/POC ratio of 0.13 (Brzezinski, 1985). The PBSi/POC ratios exceeded 0.3 during algal blooms in the Western Ross Sea and the Weddel-Scotia Sea regions (Tréguer et al., 1988; Leynaert et al., 1991). In the investigated area, the values of PBSi/POC ranged from 0.01 to 0.3 in surface waters (Figure 8A). The PBSi/POC values at St.F02 and St.F03 were close to the ratio of PBSi/POC in the pure diatom culture samples. Further, the ratios of PBSi/POC in the sea west of P07 were all greater than 0.13, with the highest value of 0.3 occurring at St.P03, which suggested that this was an area where phytoplankton were dominated by siliceous organisms. We observed that the regions where the PBSi/POC values exceed 0.13 are mainly

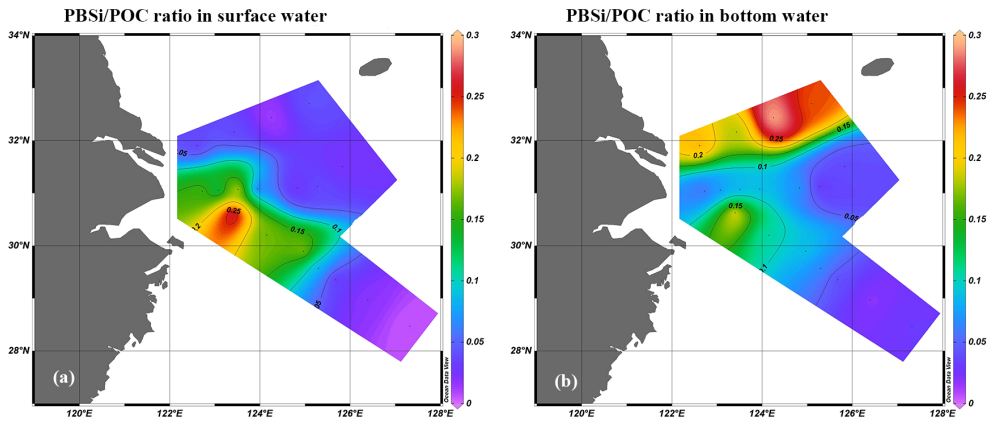

FIGURE 8
The ratios of PBSi/POC distribution in the surface **(A)** and bottom **(B)** waters of the investigated area.

concentrated in the nearshore areas of the F and PN sections, with a predominance of large-sized (>20 µm) PBSi. Therefore, the differences in PBSi size-fractionated compositions may be one of the reasons for the variations in the PBSi/POC distribution. Large-size diatoms enriched a large amount of dissolved silicate in the water column, resulting in a high PBSi/POC zone. Changes in the particle size or dominant species composition of phytoplankton can lead to differences in Si/C ratios (Tréguer et al., 1988; Boyd and Newton, 1995).

In the bottom waters, the values of PBSi/POC ranged from 0.02 to 0.29 (Figure 8B). Unlike the distribution of high-value areas in the surface layer, the high-value regions of the bottom layer are mainly concentrated in Section D. The values of PBSi/POC at St.D05, St.D07, and St.D01 were 0.30, 0.24, and 0.22, respectively. The Changjiang Diluted Water extends to the northeast toward the Tsushima/Korea Straits during summer, and the transportation and deposition of organic matter from terrestrial sources might contribute to developing high-value areas. The POC in the ECS is rapidly exported from euphotic waters, and the cross-shelf flux of POC from shelf regions to the open ocean is significant (Zhu et al., 2009). In Sections F and PN, PBSi/POC ratios showed varying decreases in depth, with the PBSi/POC ratio decreasing to 0.22 at St.P03 and below 0.13 at all other stations. This could reflect the high rates of BSi dissolution or the low rates of organic matter remineralization in the water column. According to the model estimation, approximately 75% of the BSi was dissolved in the water column, and 11% of the BSi was buried in the sediment (Liu et al., 2008). Particle size directly governs the settling velocity of particles (Berelson, 2001), and large-particle PBSi (>20 µm) might have higher sinking rates than small-particle PBSi (0.8–20 µm).

4.3 Relationship between particulate biogenic silica and the formation of hypoxia

Hypoxia is defined as DO levels below 2 or 3 mg/L (Diaz, 2001; Dai et al., 2006; Chen et al., 2007). The seasonal hypoxic zone off the Changjiang Estuary is one of the most important ecological problems in China's shelf waters, particularly in August. A trend of the gradual expansion of the hypoxic area has been observed in recent years (Li et al., 2002; Zhu et al., 2011). In order to discuss the relationship between PBSi, DO, and POC, we draw plots of PBSi versus DO and PBSi versus POC using all the data collected along sections D, F, and PN (Figure 9). The fitting line shows the negative relationship between PBSi and DO. Spearman's analysis shows a positive correlation between POC and PBSi. Stations P01 and F02 showed bottom hypoxia characteristics, with the bottom DO values distributed as 2.6 and 3.0 mg/L, respectively, and the surface and subsurface DO values in the range of 4.0–5.9 mg/L (Figure 10A). The DO saturation of each layer ranged from 16.8% to 39.4%. It is generally believed that water hypoxia is related to water column stratification, as well as oxygen depletion and the decomposition of bottom organic matter. The former is the external physical condition for hypoxia formation, and the latter is the biogeochemical endogenous cause for the formation and development of hypoxia (Justić et al., 2003; Rabalais et al., 2010). To characterize the vertical variation of Chl *a* and PBSi in water column, the concentrations of Chl *a* and PBSi at St.P01 and St.F02 were analyzed (Figure 10B). At St.F02, PBSi and Chl *a* concentrations both reached maximum values of 2.1 µmol/L and 11.6 µg/L in the surface layer, respectively. Further, with increasing depth, the concentrations of PBSi and Chl *a* decreased sharply, and DO dropped to 3 mg/L. At St.P01, closer to the coast, the values of PBSi and Chl *a* concentrations in the surface layer were 1.7 µmol/L and 0.96 µg/L. Owing to light limitation (Zhu et al., 2009), surface phytoplankton biomass was not high at St.P01; as the depth increased, the PBSi concentration reached a maximum value of 18.0 µmol/L in the 20-m layer. The bottom water of St.P01 exhibited hypoxic characteristics with a DO value of 2.6. The PBSi (diatom) dissolution is accompanied by DO depletion, and under stratified conditions in the water column, the bacterial degradation of organic substrates accelerates the dissolution of the underlying siliceous cell membranes (Abe et al., 2014). The phytoplankton of the St.P01 and St.F02 taxa were identified and

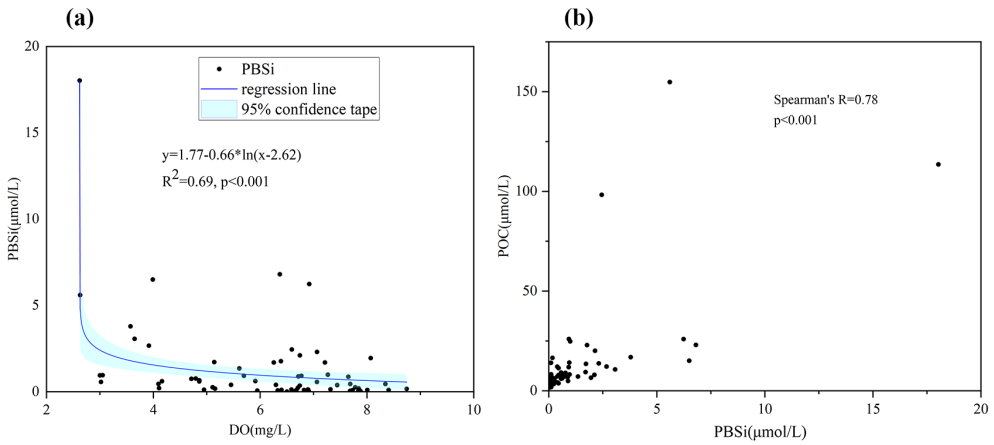

FIGURE 9
Relationships between PBSi and DO **(A)** and correlation between PBSi and POC **(B)**.

counted using a light microscope. The proportions of diatom density in the phytoplankton community both occupied an absolute dominance of more than 98% (Figure 10C). The abundance of other phytoplankton species was limited; the combined cell densities of dinoflagellates, haptophytes and chrysophytes accounted for less than 2% of the total. Additionally, the bulk stable isotope compositions ($\delta^{13}C$) of organic materials have been used to identify the source of organic matter. The $\delta^{13}C$-POC can discriminate POC sources between marine origins (−18‰ to −22‰) and terrestrial origins (−23‰ to −34‰ from C3 plants and −9‰ to −17‰ from C4 plants) (Gearing, 1988; Kumar et al., 2022). In this study, stable carbon isotope analyses, except the surface of St.P01, revealed that marine phytoplankton predominantly contributed to POC in St.P01 and St.F02. The vertical carbon isotope profiles displayed high consistency, showing less negative $\delta^{13}C$ (−20.97‰ to −23.11‰) throughout the water column at St.P01 below 10 m and at St.F02 (Figure 10D), indicating the sinking of marine particulate organic matter.

The Changjiang carries a large amount of terrestrial organic matter into the sea; however, land-sourced organic matter is generally a highly degraded product. The organic matter contains a limited quantity of nitrogenous compounds required by oxygen-consuming bacteria, making the organic matter relatively "inert" with limited oxygen-consumption capabilities (Tan et al., 1991; Tian et al., 1992). Resultantly, the formation of hypoxic zones in the bottom layer may have limited contributions from terrestrial organic matter. However, the degradation of a large amount of marine-derived organic matter, caused by the flourishing of phytoplankton, plays a significant role in the formation of hypoxic zones. Previous studies have demonstrated that the proliferation of surface diatoms can contribute 70% to 80% of bottom-layer hypoxia, as estimated based on the silicate release-to-uptake ratio (Wang et al., 2017). However, the dissolution dynamics of PBSi during sedimentation and its relationship with DO remain poorly understood. In this study, we examined the vertical distribution of PBSi in the water column and its concurrent changes with DO, providing further evidence that PBSi dissolution is accompanied by oxygen depletion during sedimentation. Our findings suggest that the proliferation of diatoms (siliceous phytoplankton) in the upper to middle water layers at stations St.P01 and St.F02 serves as the primary driver of bottom-layer hypoxia, with diatom dissolution during sedimentation closely tied to oxygen consumption.

5 Conclusion

This study systematically describes the horizontal distribution of particulate biogenic silica (PBSi) across different size fractions (>20 μm, 0.8–20 μm, and total) and its vertical distribution within the water column of the Changjiang Estuary and its adjacent waters during summer. PBSi in the 0.8–20 μm size fraction was generally dominant across sections D, F, and PN, while PBSi in the >20 μm fraction was primarily concentrated in the surface and middle waters of nearshore areas in sections F and PN (i.e., Region I). Temperature and nutrient availability were identified as critical factors influencing the size composition and spatial distribution of PBSi. For the first time, this study systematically analyzed the size composition (>20 μm, 0.8–20 μm) of PBSi in the Changjiang Estuary and adjacent areas, identified the factors affecting PBSi distribution, and examined the relationships between PBSi, particulate organic carbon (POC), and hypoxia. A more detailed size-fractionated classification provided greater accuracy in revealing the spatial distribution patterns and ecological significance of PBSi. Our findings indicated that high PBSi/POC ratios in the surface layer were predominantly concentrated in the nearshore areas of sections F and PN, with a significant contribution from large-sized (>20 μm) PBSi. However, with increasing depth, the PBSi/POC ratio declined sharply. Large-

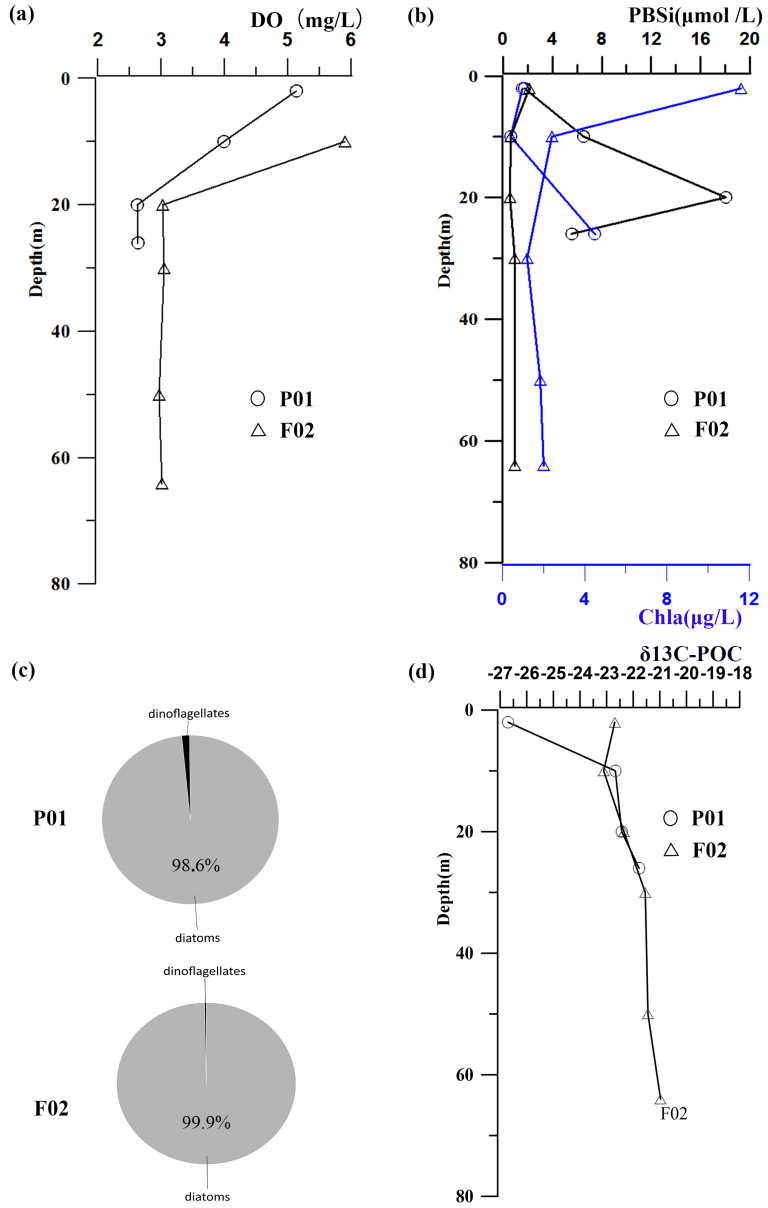

FIGURE 10
Vertical profiles of PBSi, Chlorophyll *a*, and dissolved oxygen concentrations (St.P01 and St.F02). **(A)** Dissolved oxygen concentration in the water column. **(B)** Chlorophyll *a* (blue line) and PBSi (black line) concentrations at St.P01 and St.F02. **(C)** Density ratio of diatoms and dinoflagellates in the water column (Jiang Zhibing, unpubl); the gray shading indicates diatoms, and the black shading indicates dinoflagellates. **(D)** POC carbon isotopes (δ^{13}C-POC) in the water column of St.P01 and St.F02 (Haiyan Jin, unpubl).

sized PBSi, which is capable of enriching more silicate and exhibits higher sedimentation rates, underwent substantial degradation during the sedimentation process. The grain-size structure of biogenic silica serves as a reliable indicator of biological pump efficiency. However, due to the lack of data on POC settling flux in this study, we could not address this aspect in detail. Future studies should investigate the relationships between the grain-size structure of phytoplankton populations, POC flux, and biological pump efficiency. Additionally, this study analyzed the spatial variations of dissolved oxygen (DO), PBSi, and δ^{13}C in the water column at stations St.P01 and St.F02. It confirmed that PBSi dissolution during sedimentation was accompanied by oxygen depletion. The findings highlight that the proliferation of surface diatoms and the associated oxygen consumption during their dissolution in the water column were the main drivers of bottom-layer hypoxia. This study provides new regional evidence to deepen the understanding of the interaction mechanisms between diatoms and hypoxia. In the future, greater attention should be paid to

quantifying the relationships between PBSi dissolution, silicate regeneration, and oxygen depletion. Systematic analyses are needed to evaluate the contribution of PBSi to hypoxia formation.

Data availability statement

The datasets presented in this study can be found in online repositories. The names of the repository/repositories and accession number(s) can be found in the article/Supplementary Material.

Author contributions

XL: Writing – original draft, Formal analysis, Investigation. BW: Writing – review & editing, Formal analysis, Investigation. SC: Resources, Visualization, Writing – original draft. HJ: Investigation, Writing – review & editing, Methodology. YZ: Investigation, Validation, Writing – original draft. ZJ: Formal analysis, Investigation, Writing – review & editing. HL: Funding acquisition, Methodology, Supervision, Writing – review & editing. JC: Project administration, Writing – review & editing, Conceptualization, Resources.

Funding

The author(s) declare financial support was received for the research, authorship, and/or publication of this article. This study was supported by the Natural Science Foundation of Zhejiang Province (No. LDT23D06023D06), the Open Research Program of the Key Laboratory of Marine Ecosystem Dynamic (MED), MNR (No. MED202202), the Scientific Research Fund of the Second Institute of Oceanography, MNR (No. SZ2403;JG2213), the Key R&D Program of Zhejiang (No.2023C03011), the National Key Research and Development Program of China (No.2023YFC3108000) and the National Basic Research Program of China (No.2010CB428900).

Acknowledgments

We would like to thank Prof Zhao Liang's group from ocean university of China for providing the hydrographic data. Thanks to all the staff of the research vessel "Dofanghong2" for their help during the cruise. We appreciate the data-collection assistants of Yuming Cai, Haiyan Jin, and Zhibing Jiang, all affiliated with the Second Institute of Oceanography, Ministry of Natural Resources, China.

Conflict of interest

The authors declare that the research was conducted in the absence of any commercial or financial relationships that could be construed as a potential conflict of interest.

The author(s) declared that they were an editorial board member of Frontiers, at the time of submission. This had no impact on the peer review process and the final decision.

Publisher's note

Supplementary material

The Supplementary Material for this article can be found online at: https://www.frontiersin.org/articles/10.3389/fmars.2025.1471650/full#supplementary-material

References

Abe, K., Nakagawa, N., Abo, K., and Tsujino, M. (2014). Dissolution of silica accompanied by oxygen consumption in the bottom layer of Japan's central Seto Inland Sea in summer. *J. Oceanogr.* 70, 267–276. doi: 10.1007/s10872-014-0229-5

Anderson, D. M., Kulis, D. M., Doucette, G. J., Gallagher, J. C., and Balech, E. (1994). Biogeography of toxic dinoflagellates in the genusAlexandrium from the northeastern United States and Canada. *Mar. Biol.* 120, 467–478. doi: 10.1007/BF00680222

Beardsley, R. C., Limeburner, R., Yu, H., and Cannon, G. A. (1985). Discharge of the changjiang (Yangtze river) into the East China sea. *Cont. Shelf Res.* 4, 57–76. doi: 10.1016/0278-4343(85)90022-6

Berelson, W. M. (2001). Particle settling rates increase with depth in the ocean. *Deep Sea Res. Part II: Topical Stud. Oceanography* 49, 237–251. doi: 10.1016/S0967-0645(01)00102-3

Boyd, P., and Newton, P. (1995). Evidence of the potential influence of planktonic community structure on the interannual variability of particulate organic carbon flux. *Deep Sea Res. Part I: Oceanographic Res. Papers* 42, 619–639. doi: 10.1016/0967-0637(95)00017-Z

Bryan, J. R., Rlley, J. P., and Williams, P. J. L. (1976). A winkler procedure for making precise measurements of oxygen concentration for productivity and related studies. *J. Exp. Mar. Biol. Ecol.* 21, 191–197. doi: 10.1016/0022-0981(76)90114-3

Brzezinski, M. A. (1985). The Si:C:N ratio of marine diatoms: interspecific variability and the effect of some environmental variables. *J. Physiol.* 21, 347–357. doi: 10.1111/j.0022-3646.1985.00347.x

Buesseler, K. O., Ball, L., Andrews, J., Cochran, J. K., Hirschberg, D. J., Bacon, M. P., et al. (2001). Upper ocean export of particulate organic carbon and biogenic silica in the Southern Ocean along 170°W. *Deep Sea Res. Part II: Topical Stud. Oceanography* 48, 4275–4297. doi: 10.1016/S0967-0645(01)00089-3

Cao, L., Liu, S. M., and Ren, J. (2013). Seasonal variations of particulate silicon in the Changjiang (Yangtze River) Estuary and its adjacent area. *Acta Oceanol. Sin.* 32, 1–10. doi: 10.1007/s13131-013-0293-5

Chen, C. A. (2009). Chemical and physical fronts in the Bohai, Yellow and East China seas. *J. Mar. Syst.* 78, 394–410. doi: 10.1016/j.jmarsys.2008.11.016

Chen, C., Gong, G., and Shiah, F. (2007). Hypoxia in the East China Sea: One of the largest coastal low-oxygen areas in the world. *Mar. Environ. Res.* 64, 399–408. doi: 10.1016/j.marenvres.2007.01.007

Conley, D. J. (1997). Riverine contribution of biogenic silica to the oceanic silica budget. *Limnol. Oceanogr.* 42, 774–777. doi: 10.4319/lo.1997.42.4.0774

Dai, M., Guo, X., Zhai, W., Yuan, L., Wang, B., Wang, L., et al. (2006). Oxygen depletion in the upper reach of the Pearl River estuary during a winter drought. *Mar. Chem.* 102, 159–169. doi: 10.1016/j.marchem.2005.09.020

Diaz, R. J. (2001). Overview of hypoxia around the world. *J. Environ. Qual.* 2, 275–281. doi: 10.2134/jeq2001.302275x

Gearing, J. N. (1988). *The Use of Stable Isotope Ratios for Tracing the Nearshore-Offshore Exchange of Organic Matter*. Ed. B. Jansson (Berlin, Heidelberg: Springer Berlin Heidelberg), 69–101.

Grasshoff, K., Kremling, K., and Ehrhardt, M. (2009). *Methods of Seawater Analysis*. Wiley-Vch, 159–228. doi: 10.1002/9783527613984.ch10

Harrison, P. J., Hu, M. H., Yang, Y. P., and Lu, X. (1990). Phosphate limitation in estuarine and coastal waters of China. *J. Exp. Mar. Biol. Ecol.* 140, 79–87. doi: 10.1016/0022-0981(90)90083-O

Ho, T., Pan, X., Yang, H., Wong, G. T. F., and Shiah, F. (2015). Controls on temporal and spatial variations of phytoplankton pigment distribution in the Northern South China Sea. *Deep Sea Res. Part II: Topical Stud. Oceanography* 117, 65–85. doi: 10.1016/j.dsr2.2015.05.015

Javaheri, N., Dries, R., Burson, A., Stal, L. J., Sloot, P. M. A., and Kaandorp, J. A. (2015). Temperature affects the silicate morphology in a diatom. *Sci. Rep.* 5, 11652. doi: 10.1038/srep11652

Jiang, Z., Chen, J., Zhou, F., Shou, L., Chen, Q., Tao, B., et al. (2015). Controlling factors of summer phytoplankton community in the Changjiang (Yangtze River) Estuary and adjacent East China Sea shelf. *Cont. Shelf Res.* 101, 71–84. doi: 10.1016/j.csr.2015.04.009

Justić, D., Rabalais, N. N., and Turner, R. E. (2003). Simulated responses of the Gulf of Mexico hypoxia to variations in climate and anthropogenic nutrient loading. *J. Mar. Syst.* 42, 115–126. doi: 10.1016/S0924-7963(03)00070-8

Karp-Boss, L., Boss, E., and Jumars, P. A. (1996). Nutrient fluxes to planktonic osmotrophs in the planktonic cyanobacteria Trichidesmium spp. From the Indian ocean and Caribbean and Sargasso seas. *J. Phycol.* 31, 463–477. doi: 10.1201/9780367805074-7

Kostadinov, T. S., Siegel, D. A., and Maritorena, S. (2010). Global variability of phytoplankton functional types from space: assessment via the particle size distribution. *Biogeosciences,7,10(2010-10-20)* 7, 3239–3257. doi: 10.5194/bg-7-3239-2010

Kumar, B. S. K., Vvss, S., and Cardinal, D. (2022). Tracing terrestrial versus marine sources of dissolved organic carbon in the largest monsoonal Godavari estuary in India using stable carbon isotopes. *Estuarine Coast. Shelf Sci.* 276, 108004. doi: 10.1016/j.ecss.2022.108004

Levasseur, M. E., and Therriault, J.-C. (1987). Phytoplankton biomass and nutrient dynamics in a tidally induced upwelling: the role of the NO3:SiO4 ratio. *Mar. Ecol. Prog. Ser.* 39, 87–97. doi: 10.3354/meps039087

Leynaert, A., Treguer, P., and Queguiner, B. (1991). The distribution of biogenic silicaand the composition of particulate organic matter in the Weddell-Scotia Sea duringspring1988. *Mar Chem.* 35, 435–447. doi: 10.1016/S0304-4203(09)90035-4

Li, W. K. W. (2002). Macroecological patterns of phytoplankton in the northwestern North Atlantic Ocean. *Nature* 419, 154–157. doi: 10.1038/nature00994

Li, Y., Wang, L., Fan, D., Chen, M., and Lin, Y. (2018). Distribution of biogenic silica in seafloor sediments on the East China Sea inner shelf: Seasonal variations and typhoon impact. *Estuarine Coast. Shelf Sci.* 212, 353–364. doi: 10.1016/j.ecss.2018.07.023

Li, D., Zhang, J., Huang, D., Wu, Y., and Liang, J. (2002). Oxygen depletion off the Changjiang (Yangtze River) Estuary. *Sci. China Ser. D: Earth Sci.* 45, 1137–1146. doi: 10.1360/02yd9110

Liu, S. M., Qi, X. H., Li, X., Ye, H. R., Wu, Y., Ren, J. L., et al. (2016a). Nutrient dynamics from the Changjiang (Yangtze River) estuary to the East China Sea. *J. Mar. Syst.* 154, 15–27. doi: 10.1016/j.jmarsys.2015.05.010

Liu, S. M., Ye, X. W., Zhang, J., Zhang, G. S., and Wu, Y. (2008). The silicon balance in Jiaozhou Bay, North China. *J. Mar. Syst.* 74, 639–648. doi: 10.1016/j.jmarsys.2008.06.001

Liu, J., Zang, J., Bouwman, L., Liu, S., Yu, Z., and Ran, X. (2016b). Distribution and budget of dissolved and biogenic silica in the Bohai Sea and Yellow Sea. *Biogeochemistry* 130, 85–101. doi: 10.1007/s10533-016-0244-2

Liu, S. M., Zhang, J., and Li, R. (2005). Ecological significance of biogenic silica in the East China Sea. *Mar. Ecology-Progress Ser.* 290, 15–26. doi: 10.3354/meps290015

Lomas, M. W., and Glibert, P. M. (1999). Temperature regulation of nitrate uptake: a novel hypothesis about nitrate uptake and reduction in cool-water diatoms. *Limnol. Oceanogr.* 44, 556–572. doi: 10.4319/lo.1999.44.3.0556

Maranon, E., Holligan, P. M., Barciela, R., González, N., and Varela, M. (2001). Patterns of phytoplankton size structure and productivity in contrasting open-ocean environments. *Mar. Ecol. Prog.* 216, 43–56. doi: 10.3354/meps216043

Nelson, D. M., Anderson, R. F., Barber, R. T., Brzezinski, M. A., Buesseler, K. O., Chase, Z., et al. (2002). Vertical budgets for organic carbon and biogenic silica in the Pacific sector of the Southern Ocean 1996–1998. *Deep Sea Res. Part II: Topical Stud. Oceanography* 49, 1645–1674. doi: 10.1016/S0967-0645(02)00005-X

Nelson, D. M., Tréguer, P., Brzezinski, M. A., Leynaert, A., and Quéguiner, B. (1995). Production and dissolution of biogenic silica in the ocean: Revised global estimates, comparison with regional data and relationship to biogenic sedimentation. *Glob. Biogeochem. Cycle* 9, 359–372. doi: 10.1029/95GB01070

Rabalais, N. N., Diaz, R. J., and Levin, L. A. (2010). Dynamics and distribution of natural and human caused hypoxia. *Biogeo Sci.* 7, 585–619. doi: 10.5194/bg-7-585-2010

Ragueneau, O., Savoye, N., Del Amo, Y., Cotten, J., Tardiveau, B., and Leynaert, A. (2005). A new method for the measurement of biogenic silica in suspended matter of coastal waters: using Si : Al ratios to correct for the mineral interference. *Cont. Shelf Res.* 25, 697–710. doi: 10.1016/j.csr.2004.09.017

Savidge, G., Boyd, P., Pomroy, A., Harbour, D., and Joint, I. (1995). Phytoplankton production and biomass estimates in the northeast Atlantic Ocean, May–June 1990. *Deep Sea Res. Part I: Oceanographic Res. Papers* 42, 599–617. doi: 10.1016/0967-0637(95)00016-Y

Su, J. (1998). Circulation dynamics of the China seas north 18°N. *Sea* 11, 483–505.

Tan, F. C., Cai, D. L., and Edmond, J. M. (1991). Carbon isotope geochemistry of the Changjiang estuary. *Estuarine Coast. Shelf Sci.* 32, 395–403. doi: 10.1016/0272-7714(91)90051-C

Tian, R. C., Sicre, M. A., and Saliot, A. (1992). Aspects of the geochemistry of sedimentary sterols in the Chang Jiang estuary. *Org. Geochem.* 18, 843–850. doi: 10.1016/0146-6380(92)90052-Y

Tréguer, P., Gueneley, S., and Kamatani, A. (1988). Biogenic silica and particulate organic matter from the Indian sector of the Southern Ocean. *Mar. Chem.* 23, 167–180. doi: 10.1016/0304-4203(88)90030-8

Tréguer, P., Nelson, D. M., Van Bennekom, A. J., Demaster, D. J., Leynaert, A., and Quéguiner, B. (1995). The silica balance in the world ocean: a reestimate. *Science* 268, 375–379. doi: 10.1126/science.268.5209.375

Tréguer, P., and Pondaven, P. (2000). Global change. Silica control of carbon dioxide. *Nature* 406, 358–359. doi: 10.1038/35019236

Wang, B., Chen, J., Jin, H., Li, H., Huang, D., and Cai, W. (2017). Diatom bloom-derived bottom water hypoxia off the Changjiang estuary, with and without typhoon influence. *Limnol. Oceanogr.* 62, 1552–1569. doi: 10.1002/lno.10517

Wang, H., Dai, M., Liu, J., Kao, S., Zhang, C., Cai, W., et al. (2016). Eutrophication-driven hypoxia in the East China sea off the Changjiang estuary. *Environ. Sci. Technol.* 50, 2255–2263. doi: 10.1021/acs.est.5b06211

Wang, L., Fan, D., Li, W., Liao, Y., Zhang, X., Liu, M., et al. (2014). Grain-size effect of biogenic silica in the surface sediments of the East China Sea. *Cont. Shelf Res.* 81, 29–37. doi: 10.1016/j.csr.2014.03.005

Xiao, W., Liu, X., Irwin, A. J., Laws, E. A., Wang, L., Chen, B., et al. (2018). Warming and eutrophication combine to restructure diatoms and dinoflagellates. *Water Res.* 128, 206–216. doi: 10.1016/j.watres.2017.10.051

Zhang, J., Liu, S. M., Ren, J. L., Wu, Y., and Zhang, G. L. (2007). Nutrient gradients from the eutrophic Changjiang (Yangtze River) Estuary to the oligotrophic Kuroshio waters and re-evaluation of budgets for the East China Sea Shelf. *Prog. Oceanogr.* 74, 449–478. doi: 10.1016/j.pocean.2007.04.019

Zhou, P., Song, X., Yuan, Y., Cao, X., Wang, W., Chi, L., et al. (2018). Water mass analysis of the East China sea and interannual variation of Kuroshio subsurface water intrusion through an optimum multiparameter method. *J. Geophysical Research: Oceans* 123, 3723–3738. doi: 10.1029/2018JC013882

Zhu, Z., Ng, W., Liu, S. M., Zhang, J., Chen, J., and Wu, Y. (2009). Estuarine phytoplankton dynamics and shift of limiting factors: a study in the Changjiang (Yangtze River) Estuary and adjacent area. *Estuarine Coast. Shelf Sci.* 84, 393–401. doi: 10.1016/j.ecss.2009.07.005

Zhu, Z., Zhang, J., Wu, Y., Zhang, Y., Lin, J., and Liu, S. (2011). Hypoxia off the Changjiang (Yangtze River) Estuary: Oxygen depletion and organic matter decomposition. *Mar. Chem.* 125, 108–116. doi: 10.1016/j.marchem.2011.03.005